Journal of Advanced Research 25 (2020) 87–96

Contents lists available at ScienceDirect

Journal of Advanced Research

journal homepage: www.elsevier.com/locate/jare

Composite learning sliding mode synchronization of chaotic fractional-order neural networks

Zhimin Han [a], Shenggang Li [a], Heng Liu [b,*]

[a] College of Mathematics and Information Science, Shaanxi Normal University, Xi'an 710119, China
[b] School of Science, Guangxi University for Nationalities, Nanning 530006, China

HIGHLIGHTS

- A sliding surface extending from integer-order to fractional-order is introduced.
- The stability of FONNs is analyzed by means of the Lyapunov function.
- A composite learning law is designed for FONNs under the IE condition.

GRAPHICAL ABSTRACT

Parameter estimations for SMC and CLSMC.

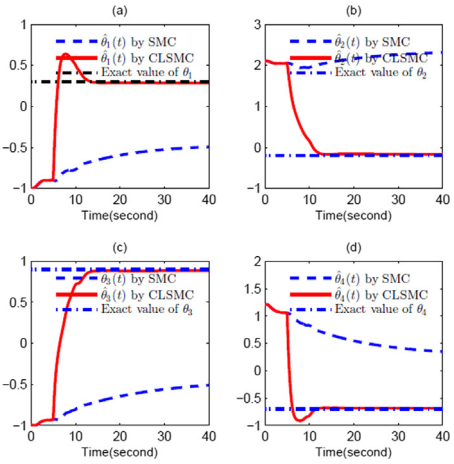

ARTICLE INFO

Article history:
Received 21 January 2020
Revised 3 April 2020
Accepted 13 April 2020
Available online 26 April 2020

Keywords:
Composite learning
Fractional-order neural network
Sliding mode control
Interval excitation

ABSTRACT

In this work, a sliding mode control (SMC) method and a composite learning SMC (CLSMC) method are proposed to solve the synchronization problem of chaotic fractional-order neural networks (FONNs). A sliding mode surface and an adaptive law are constructed to update parameter estimation. The SMC ensures that the synchronization error asymptotically tends to zero under a strict permanent excitation (PE) condition. To reduce its rigor, online recording data together with instantaneous data is used to define a prediction error about the uncertain parameter. Both synchronization error and prediction error are used to construct a composite learning law. The proposed CLSMC method can ensure that the synchronization error asymptotically approaches zero, and it can accurately estimate the uncertain parameter. The above results obtained in the CLSMC method only requires an interval-excitation (IE) condition which can be easily satisfied. Finally, comparative results reveal the control effects of the two proposed methods.

Peer review under responsibility of Cairo University.

* Corresponding author.
E-mail address: liuheng122@gmail.com (H. Liu).

https://doi.org/10.1016/j.jare.2020.04.006
2090-1232/

Introduction

Fractional calculus has a history of more than 300 years. Recently, fractional calculus as an important part of mathematics, has been studied by more and more scientists [1,2]. Fractional-order systems that are described by fractional-order differential formulas have applications in different fields, such as bioengineering, thermal diffusion, electronics, robotics, and physics [3–7]. The fractional calculus has some unique properties including memory and inheritance, which are useful to model nonlinear systems. Therefore, many scientists apply fractional-order calculus to neural networks (NNs) to construct fractional-order NNs (FONNs), with the goal of showing more clearly the dynamic behavior of neurons in NNs. In [8], Arena et al. gave a fractional-order cellular NNs. In [9], Petráč introduced a fractional-order 3-cell network to show the limit cycle and stable orbit under variable parameters. In addition, FONNs have important applications in parameter estimation domain [10,11]. It has been shown bifurcations and chaos exist in FONNs [8,12]. A fractional-order Hopfield neural model was analyzed in [13], and the stability of this model was studied by using energy-like functions. The synchronization problem of fractional-order chaotic NNs was analyzed by means of Mittag-Leffler function and linear feedback control in [14], fractional-order chaotic systems was investigated by means of adaptive fuzzy synchronization control based on backstepping in [15,16] and the adaptive synchronization problem of uncertain FONNs was studied by using the Lyapunov approach in [17]. Some interesting control methods are proposed for FONN in above literature, however, the mismatched unknown parameters are not considered. If mismatched parameters appear in a FONN, these methods may not have good control performance. Therefore, it is worthwhile to find a good method to solve this problem.

Among many usually used control methods, sliding mode control (SMC) has been studied by more and more scholars in recent years [18–21]. The SMC method is an effective robust nonlinear control strategy, one of its main characteristics is the switch of control law, to make the system transfer from the initial state to the set sliding surface, so that the system has good stability, tracking ability and anti-interference ability on the sliding surface. It is well known in the past that the SMC method was mostly used in integer-order nonlinear systems. The important role of SMC was demonstrated in [22,23]. Now, many scientists have extended the SMC methods to fractional-order systems, for example, MIMO nonlinear fractional-order systems [24], fractional-order chaotic systems [17,25], and FONNs [26]. However, in these control methods, the SMC can only ensure that the parameters are convergent, that is, the accurate estimations of these parameters can not be guaranteed. Therefore, how to find a effective method to estimate the parameters accurately during designing SMC for fractional-order systems is a meaningful work.

Composite adaptive control (CAC) was introduced in [27] to obtain accurate parameter estimation by using tracking errors and constructing prediction errors. One of the important functions of the CAC is that it can improve the parameter convergence speed and estimate parameters more accurately. The latest results about CAC can be seen in [28–32]. The CAC method has better control capability than the traditional adaptive control method that the permanent excitation (PE) condition is required in order for parameter estimates to converge. To eliminate this limitation, the composite learning methods were introduced in [33–36]. In the composite learning, online recorded data generated during control process is used to designed the prediction error, which is then combined with the tracking error to produce a composite learning law. The composite learning method is crucial to ensure that accurate parameter estimation are obtained under an interval-excitation (IE) condition which is lower than the PE condition. However, the composite learning control methods previously seen are extensively used in integer-order nonlinear systems. With respect to fractional-order systems, some preliminary works have been done, for example, in [18,37]. A composite learning adaptive dynamic surface was used to study fractional-order nonlinear systems (FONSs) in [37] and composite learning adaptive SMC was used to study FONSs in [18]. The above two works provide a clear idea to use composite learning method to analyze the control of FONSs in the future. Whereas, in [18,37], only SISO systems are considered. Therefore, it is necessary and challenging to apply composite learning to synchronize MIMO FONNs.

Based on above analysis, this work considers the synchronization control for a class of FONNs through SMC and CLSMC. First, a sliding surface is introduced, and then a traditional SMC is shown to ensure that the synchronization error asymptotically approaches zero. In order to get exact errors of the uncertain parameters, a CLSMC method is proposed. The stability studies for the SMC and the CLSMC methods is proved by the integral-order Lyapunov stability criteria. Last but not least, the control capability of the two methods is compared through theoretical analysis and simulation results. Compared to some previous works, such as [18,37], the contributions of this study contain: (1) A sliding surface extending from integer-order to fractional-order is introduced; (2) The stability of FONNs is analyzed by means of the Lyapunov function; (3) A composite learning law is defined to design the CLSMC for FONNs. The convergence of synchronization errors and the accuracy of parameter estimation in FONNs are sufficient to ensured under the IE condition is lower than the PE condition. Compared with the traditional SMC, the CLSMC method has better control ability and can estimate parameter more accurately.

The article is divided into the following parts. Some of the fractional-order calculus preliminaries are given in Section "Preliminaries". Section "Adaptive sliding mode control design" gives the description of the problem, fractional sliding surface design, the concepts of IE and PE, and the construction of the SMC and CLSMC. Section "Simulation example" shows the simulation example to compare the effects of the SMC method and the CLSMC method. Finally, Section "Conclusions" concludes this work.

Preliminaries

Fractional-order calculus is an extension of integer-order calculus, and the definition of Caputo's fractional-order calculus will be used in the following discussion. The definition of α-th fractional-order integral is

$$I_t^{\alpha} f(t) = \frac{1}{\Gamma(\alpha)} \int_0^t (t-\varrho)^{\alpha-1} f(\varrho) d\varrho, \tag{1}$$

where $\Gamma(s) = \int_0^{\infty} t^{s-1} e^{-t} dt$.

The Caputo's fractional-order differential is

$$D_t^{\alpha} f(t) = \frac{1}{\Gamma(n-\alpha)} \int_0^t (t-\varrho)^{n-\alpha-1} f^{(n)}(\varrho) d\varrho, \tag{2}$$

where $\alpha > 0$, and $n-1 \leqslant \alpha < n$. For ease of use, we will assume that $0 < \alpha < 1$ hereafter. Therefore, (2) is expressed as

$$D_t^{\alpha} f(t) = \frac{1}{\Gamma(1-\alpha)} \int_0^t (t-\varrho)^{-\alpha} f\prime(\varrho) d\varrho. \tag{3}$$

Lemma 1. *If $x(t) \in C^1[0,T]$ for some $T > 0$, then it holds:*

$$I_t^{\alpha} D_t^{\alpha} x(t) = x(t) - x(0), \tag{4}$$

and

$$D_t^{\alpha} I_t^{\alpha} x(t) = x(t). \tag{5}$$

Lemma 2. *Caputo's fractional calculus satisfies*

$$D_t^{\alpha}(\lambda v_1(t) + \mu v_2(t)) = \lambda D_t^{\alpha} v_1(t) + \mu D_t^{\alpha} v_2(t), \tag{6}$$

where λ , $\mu \in \mathcal{R}$.

Adaptive sliding mode control design

Problem statement

The dynamics of fractional-order cellular NNs are written as the following differential equations:

$$D_t^{\alpha} \zeta_i(t) = -a_i \zeta_i(t) + \sum_{j=1}^{n} b_{ij}(t) f_j(\zeta_j(t)) + H_i + \psi_i^T(\zeta(t))\theta, \tag{7}$$

where $i = 1, 2, \cdots, n$, α is the fractional order, n is the number of units in the NN, $\zeta_i(t)$ represents the state of the i-th unit at time t, $b_{ij}(t)$ is the connection weight of the j-th neuron on the i-th neuron which is assumed to be disturbed, $f_j(\zeta)$ is a nonlinear function, a_i corresponds to the rate with which the neuron will reset its potential to the resting state when disconnected from the network, H_i represents the external input, $\psi_i : \mathcal{R}^i \mapsto \mathcal{R}^m$ with $m \in \mathcal{N}$ is a known vector function, and $\theta \in \mathcal{R}^m$ is an unknown constant vector to be estimated.

According to the concept of driver-response, we set the system (7) as the drive FONN, and consider the response FONN as:

$$D_t^{\alpha} \eta_i(t) = -a_i \eta_i(t) + \sum_{j=1}^{n} b_{ij}(t) f_j(\eta_j(t)) + H_i + u_i(t), \tag{8}$$

where $i = 1, 2, \cdots, n$, $\eta_i(t)$ is the state vector of the response system, $u_i(t)$ is the control input.

Definition 1. A signal $\psi(t)$ is of IE on $[T - \varsigma_0, T]$ for $\varsigma_0 > 0$ and $T > \varsigma_0$ iff $\int_{T-\varsigma_0}^{T} \psi^T(\varsigma)\psi(\varsigma)d\varsigma \geqslant vI_{c\times c}$ where $v \in \mathcal{R}^+$.

Definition 2. A signal $\psi(t)$ is of PE iff $\int_{t-\varsigma_0}^{t} \psi^T(\varsigma)\psi(\varsigma)d\varsigma \geqslant vI_{c\times c}$ for $v \in \mathcal{R}^+, \varsigma_0 > 0$ and all $t \in \mathcal{R}^+$.

There are two indices that are usually used to describe the control performance, i.e., the integral squared error (ISE) and the mean squared error (MSE), which can be defined as follows.

The ISE:

$$ISE = \int_0^{\infty} \underline{e}^2(t)dt. \tag{9}$$

The MSE:

$$MSE = \int_0^{\infty} t\underline{e}^2(t)dt, \tag{10}$$

where $\underline{e}(t)$ is the error between the actual output and the expected output.

Adaptive sliding mode control and stability analysis

The synchronization error is defined as:

$$e(t) = \eta(t) - \zeta(t). \tag{11}$$

The parameter estimation error is expressed by

$$\tilde{\theta}(t) = \hat{\theta}(t) - \theta, \tag{12}$$

with $\hat{\theta}(t)$ being the evaluation of θ. The error dynamics between the response system (8) and the drive system (7) can be written as:

$$D_t^{\alpha} e_i(t) = -a_i e_i(t) + \sum_{j=1}^{n} b_{ij}(t)[f_j(\eta_j(t)) - f_j(\zeta_j(t))] + u_i(t) - \psi_i^T(\zeta(t))\theta. \tag{13}$$

In this part, a sliding mode control method with adaptive law of $\hat{\theta}(t)$ is proposed to ensure the convergence of synchronization error $e(t)$ and parameter estimation error $\tilde{\theta}(t)$. Here we will introduced the following fractional sliding surface:

$$S_i(t) = \delta_i I_t^{1-\alpha} e_i(t), \tag{14}$$

where δ_i is chosen such that $S_i(t)$ converges quickly. As an extension of the integral sliding surface, the fractional sliding surface (14) is the same as integral SMC, so the control action can be realized through two steps: the system state variables goes into the sliding surface and then stays on it.

It follows from (14) that

$$\begin{aligned} \dot{S}_i(t) &= \delta_i D_t^{\alpha} e_i(t) \\ &= \delta_i \left[-a_i e_i(t) + \sum_{j=1}^{n} b_{ij}(t) \left[f_j(\eta_j(t)) - f_j(\zeta_j(t)) \right] + u_i(t) - \psi_i^T(\zeta(t))\theta \right]. \end{aligned} \tag{15}$$

Then, the control input $u_i(t)$ can be given as

$$\begin{aligned} u_i(t) = a_i e_i(t) - \sum_{j=1}^{n} b_{ij}(t) \left[f_j(\eta_j(t)) - f_j(\zeta_j(t)) \right] + \psi_i^T(\zeta(t))\hat{\theta}(t) \\ - \frac{1}{\delta_i} \lambda S_i(t), \end{aligned} \tag{16}$$

where $\lambda \in \mathcal{R}^+$.

We will use the following equation to update $\hat{\theta}$:

$$\mathsf{F}(t) = -\gamma \sum_{i=1}^{n} \delta_i \psi_i(\zeta(t)) S_i(t), \dot{\hat{\theta}}(t) = \Lambda(\hat{\theta}(t), \mathsf{F}(t)), \tag{17}$$

where $\gamma \in \mathcal{R}^+$, and $\Lambda(\hat{\theta}(t), \mathsf{F}(t))$ is designed by

$$\Lambda(\hat{\theta}(t), \mathsf{F}(t)) = \begin{cases} \mathsf{F}(t), & \text{if } \|\hat{\theta}(t)\| \leqslant \beta, \\ \mathsf{F}(t) + \frac{\hat{\theta}(t)\hat{\theta}^T(t)\mathsf{F}(t)}{\|\hat{\theta}(t)\|^2}, & \text{otherwise}, \end{cases} \tag{18}$$

where $\beta > 0$.

Thus, according to the above calculation, we can get the following conclusions.

Theorem 1. *With regard to the drive FONN (7) and the response FONN (8). The sliding mode controller (16) and the adaptive law (17) can not only make all signals keep bounded but also make the synchronization error $e(t)$ asymptotically tend to the origin.*

Proof. Substituting the control input (16) into (15) yields

$$\begin{aligned} \dot{S}_i(t) &= \delta_i \left[\psi_i^T(\zeta(t))\hat{\theta}(t) - \psi_i^T(\zeta(t))\theta - \tfrac{1}{\delta_i}\lambda S_i(t) \right], \\ &= -\lambda S_i(t) + \delta_i \psi_i^T(\zeta(t))\tilde{\theta}(t). \end{aligned} \tag{19}$$

The lyapunov function is set to be:

$$V(t) = \frac{1}{2} \sum_{i=1}^{n} S_i^2(t) + \frac{1}{2\gamma} \tilde{\theta}^T(t)\tilde{\theta}(t). \tag{20}$$

Differentiating the Lyapunov function (20) gives

$$\dot{V}(t) = \sum_{i=1}^{n} S_i(t)\dot{S}_i(t) + \frac{1}{\gamma}\tilde{\theta}^T(t)\dot{\tilde{\theta}}(t). \tag{21}$$

Substituting (19) into (21) yields

$$\begin{aligned}\dot{V}(t) &= \sum_{i=1}^{n} S_i(t)[-\lambda S_i(t) + \delta_i\psi_i^T(\zeta(t))\tilde{\theta}(t)] + \tfrac{1}{\gamma}\tilde{\theta}^T(t)\dot{\tilde{\theta}}(t),\\ &= -\lambda\sum_{i=1}^{n} S_i^2(t) + \sum_{i=1}^{n}\delta_i\psi_i^T(\zeta(t))\tilde{\theta}(t)S_i(t) + \tfrac{1}{\gamma}\tilde{\theta}^T(t)\dot{\tilde{\theta}}(t),\\ &= -\lambda\sum_{i=1}^{n} S_i^2(t) + \tilde{\theta}^T(t)\left[\sum_{i=1}^{n}\delta_i\psi_i(\zeta(t))S_i(t) + \tfrac{1}{\gamma}\dot{\tilde{\theta}}(t)\right].\end{aligned} \tag{22}$$

Using [38, Th.4.6.1], and substituting (17) into (22) yields

$$\begin{aligned}\dot{V}(t) &\leqslant -\lambda\sum_{i=1}^{n} S_i^2(t) + \tilde{\theta}^T(t)\left[\sum_{i=1}^{n}\delta_i\psi_i(\zeta(t))S_i(t) + \tfrac{1}{\gamma}\left[-\gamma\sum_{i=1}^{n}\delta_i\psi_i(\zeta(t))S_i(t)\right]\right],\\ &= -\lambda\sum_{i=1}^{n} S_i^2(t).\end{aligned} \tag{23}$$

Thus, asymptotic stability of the controlled system is achieved, and this ends the proof of Theorem 1. □

Composite learning sliding mode control and stability analysis

From the above SMC design, we known that the adaptation law (17) consists of instantaneous data related to $S_i(t)$, and its value is used to update $\hat{\theta}(t)$ online. In (19), $\lambda, S_i(t), \delta_i$ and $\psi_i^T(\zeta(t))$ are available. When $\dot{S}_i(t)$ is also available, the $\tilde{\theta}(t)$ can be calculated, which gives an accurate estimation of $\hat{\theta}(t)$. Later in this article, a CLSMC method will be provided to guarantee not only that $e(t)$ asymptotically approaches zero without the PE condition but also obtain the accurate estimation of θ. To meet above objectives, we set the prediction error as

$$\epsilon_i(t) = h_i(\zeta(t))\tilde{\theta}(t), \tag{24}$$

with $h_i(\zeta(t)) : \mathbb{R}^n \mapsto \mathbb{R}^{m\times m}$ being expressed as

$$h_i(\zeta(t)) = \begin{cases} \mathbf{0}_{m\times m}, & \text{for } t \leqslant \varsigma_0,\\ \int_{t-\varsigma_0}^{t}\Psi_i(\zeta(\varsigma))\Psi_i^T(\zeta(\varsigma))d\varsigma, & \text{for } t > \varsigma_0,\end{cases} \tag{25}$$

with $\Psi_i(\zeta(t)) = \delta_i\psi_i(\zeta(t))$. Then, we will use the following equation to update $\hat{\theta}$:

$$\begin{cases} \mathsf{F}(t) = -\gamma\left[\sum_{i=1}^{n}\delta_i\psi_i(\zeta(t))S_i(t) + \sum_{i=1}^{n}\omega\epsilon_i(t)\right],\\ \dot{\hat{\theta}}(t) = \Lambda(\hat{\theta}(t), \mathsf{F}(t)),\end{cases} \tag{26}$$

where $\omega > 0$ is a learning parameter, and $\Lambda(\hat{\theta}(t), \mathsf{F}(t))$ has the same concept as (18). According to (25), the definition of IE condition is rewritten as $h_i(\zeta(t)) \geqslant vI$ with v being an exciting term. Let T_1 ($T_1 > \varsigma_0$) be the first point that satisfies Definition 1, exciting term that varies over time is

$$v_d(t) = \sup_{\varsigma\in[T_1,t]}\{v(t)\}.$$

A graph of $v(t)$ and $v_d(t)$ can be indicated as Fig. 1, in which $v_d(t)$ is defined as

$$v_d(t) = \begin{cases} 0, & t \in [0, T_1),\\ v(t), & t \in [T_1, T_2),\\ v(T_2), & t \in [T_2, T_3),\\ v(t), & t \in [T_3, T_4),\\ v(T_4), & t \in [T_4, \infty).\end{cases}$$

Next, we will calculate the value of $\epsilon_i(t)$. Let

$$\varepsilon_i(t) = \int_{t-\varsigma_0}^{t}\Psi_i(\zeta(\varsigma))\Psi_i^T(\zeta(\varsigma))\theta d\varsigma. \tag{27}$$

Since $\Psi_i(\zeta(t)) = \delta_i\psi_i(\zeta(t))$, Eq. (19) is equivalent to

$$\dot{S}_i(t) = -\lambda S_i(t) + \Psi_i^T(\zeta(t))\tilde{\theta}(t). \tag{28}$$

Multiply both ends of (28) by $\Psi_i(\zeta(t))$

$$\Psi_i(\zeta(t))\dot{S}_i(t) = -\lambda\Psi_i(\zeta(t))S_i(t) + \Psi_i(\zeta(t))\Psi_i^T(\zeta(t))\tilde{\theta}(t). \tag{29}$$

According to (12), Eq. (29) is written as

$$\begin{aligned}\Psi_i(\zeta(t))\dot{S}_i(t) &= -\lambda\Psi_i(\zeta(t))S_i(t) + \Psi_i(\zeta(t))\Psi_i^T(\zeta(t))[\hat{\theta}(t) - \theta],\\ &= -\lambda\Psi_i(\zeta(t))S_i(t) + \Psi_i(\zeta(t))\Psi_i^T(\zeta(t))\hat{\theta}(t) - \Psi_i(\zeta(t))\Psi_i^T(\zeta(t))\theta.\end{aligned} \tag{30}$$

From the above formula, we can get

$$\begin{aligned}\Psi_i(\zeta(t))\Psi_i^T(\zeta(t))\theta = &-\Psi_i(\zeta(t))\dot{S}_i(t) - \lambda\Psi_i(\zeta(t))S_i(t)\\ &+ \Psi_i(\zeta(t))\Psi_i^T(\zeta(t))\hat{\theta}(t).\end{aligned} \tag{31}$$

Consequently, (27) and (31) imply

$$\varepsilon_i(t) = \int_{t-\varsigma_0}^{t}\Psi_i(\zeta(\varsigma))\left[-\dot{S}_i(\varsigma) - \lambda S_i(\varsigma) + \Psi_i^T(\zeta(\varsigma))\hat{\theta}(\varsigma)\right]d\varsigma. \tag{32}$$

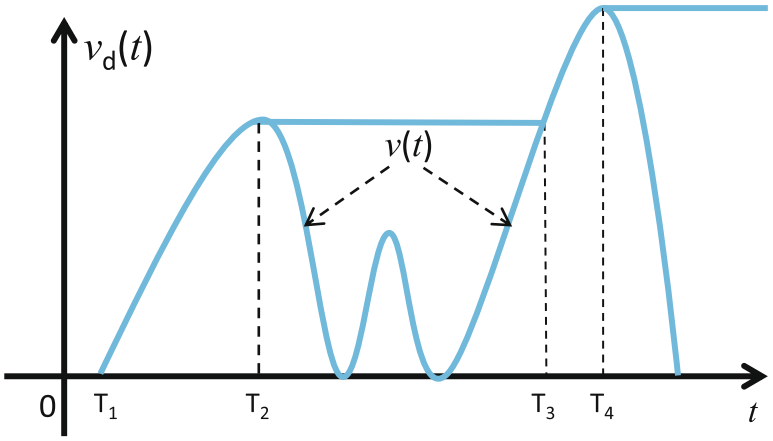

Fig. 1. A diagram of $v(t)$ and $v_d(t)$.

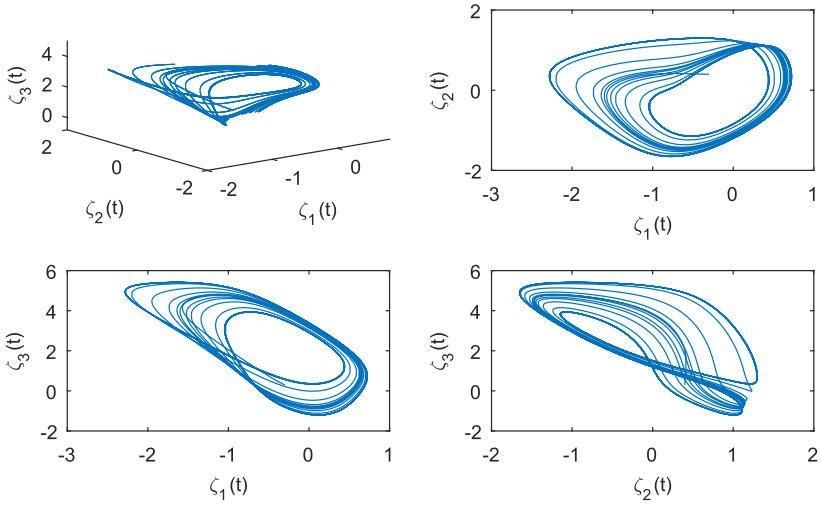

Fig. 2. Dynamical behavior of system (38) with initial value $[-0.3, 0.4, 0.3]^T$.

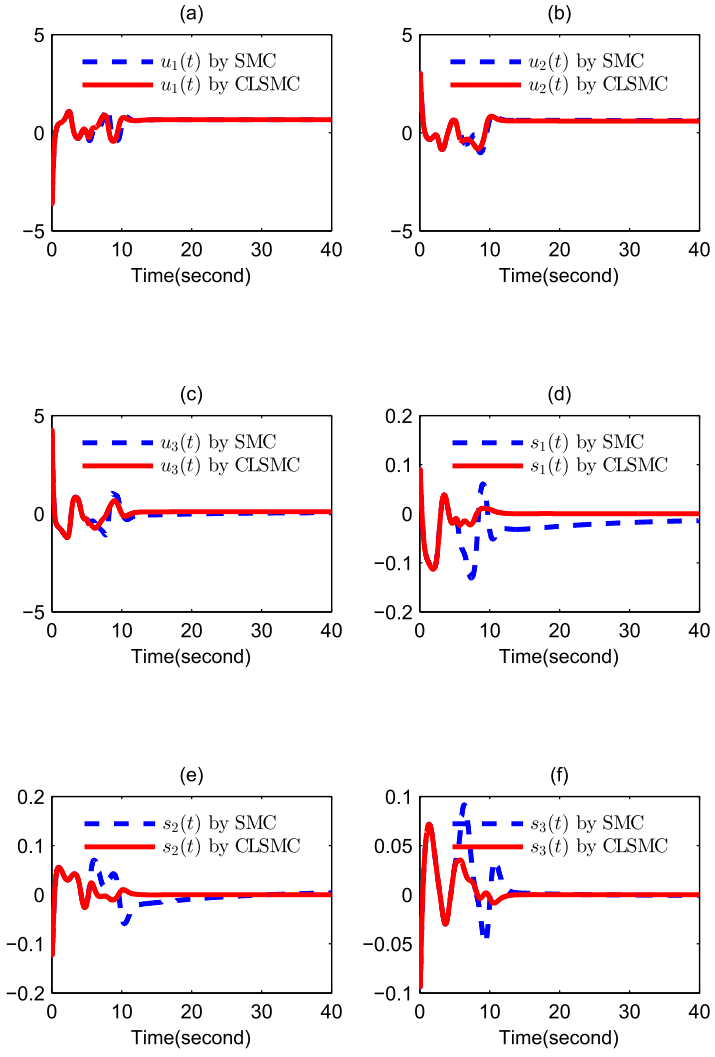

Fig. 3. Control inputs and sliding surfaces under SMC and CLSMC.

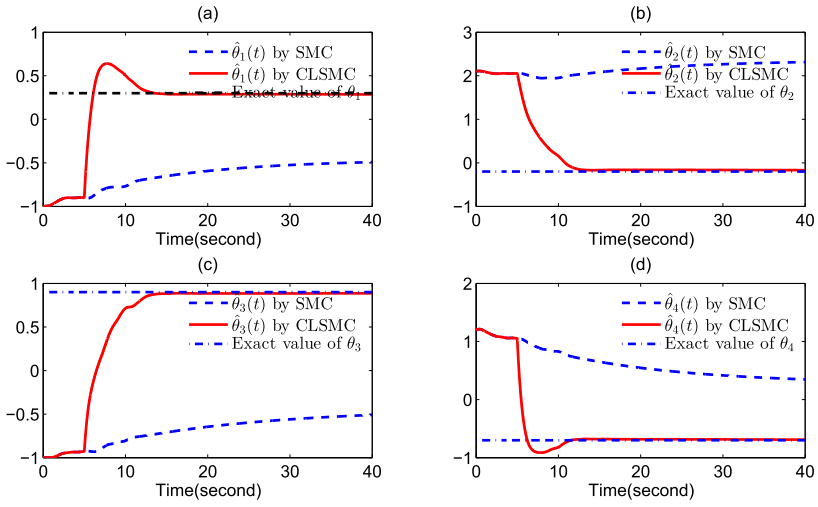

Fig. 4. Parameter estimations for SMC and CLSMC.

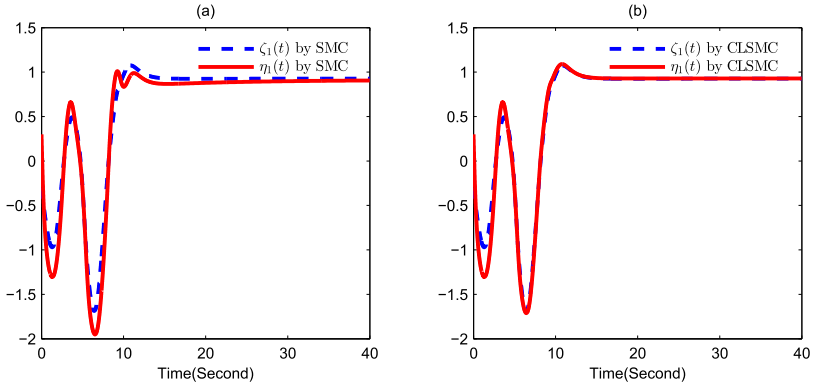

Fig. 5. Synchronization between $\zeta_1(t)$ and $\eta_1(t)$ for SMC and CLSMC.

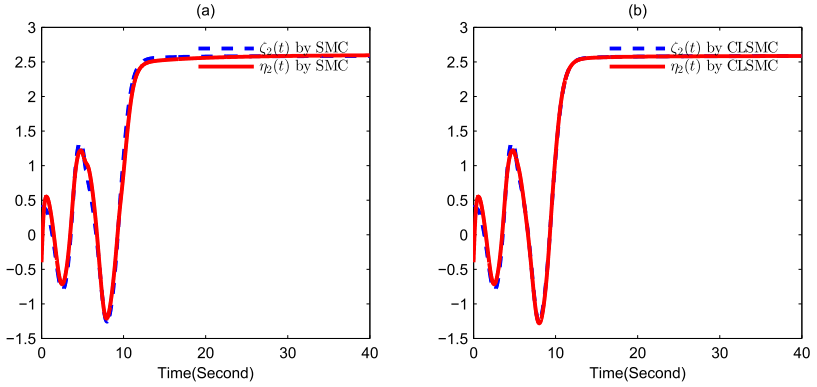

Fig. 6. Synchronization between $\zeta_2(t)$ and $\eta_2(t)$ for SMC and CLSMC.

So $\epsilon_i(t)$ is calculated as

$$\epsilon_i(t) = h_i(\zeta(t))\hat{\theta}(t) - \int_{t-\varsigma_0}^{t} \Psi_i(\zeta(\varsigma))\left[-\dot{S}_i(\varsigma) - \lambda S_i(\varsigma) + \Psi_i^T(\zeta(\varsigma))\hat{\theta}(\varsigma)\right]d\varsigma. \quad (33)$$

Remark 1. In the SMC method, only instantaneous data is applied to update the parameter estimator (see, the adaptation law (17)). However, in the CLSMC method, the combination of online recording data and instantaneous data is used to update the parameter estimator.

Remark 2. The composite learning law (26) is constructed under the IE condition by using prediction error (24). In this law all recorded data on the interval $t \in [0, +\infty)$ is used to get an accurate estimate of unknown parameter θ. In (25), ς_0 can be selected according to the control target, but if ς_0 is too large, it puts a great quantity of memory pressure on the system. The control rate of CLSMC will vary with the change of γ and ω, but if γ and ω are too big, the results are not ideal. In fact, in our work, we can use not too large parameters (see the simulation in Section "Simulation example") to obtain good synchronization performance. That is, the proposed CLSMC method is meaningful and realistic.

Remark 3. In the CLSMC design, a main problem need to be solved is how to obtain the prediction error. Here, we will give a procedure to elaborate how to calculate $\epsilon_i(t)$. In Definition 1, if $h_i(\zeta(t)) \leqslant vI, h_i(\zeta(t))$ is $\mathbf{0}$. At this point, $\epsilon_i(t) = \mathbf{0}$. On the other hand, if $h_i(\zeta(t)) > vI$, and all the data in the interval $[T - \varsigma_0, T]$ is used to calculate the prediction error $\epsilon_i(t)$ by

$$\epsilon_i(t) = h_i(\zeta(t))\hat{\theta}(t) - \varepsilon_i(t). \tag{34}$$

Noting that the exact value of $\dot{S}_i(t)$ is not available, to obtain $\varepsilon_i(t)$ in (32), we can use the data of $S_i(t)$. For example, it can be computed as

$$\dot{S}_i(t) \approx \frac{S_i(t + \triangle t) - S_i(t)}{\triangle t}, \tag{35}$$

where the estimation error $o(\triangle t)$. On the other hand, in the CLSMC design, the integral is used in (27), which can further reduce the calculation error of $\varepsilon_i(t)$.

Theorem 2. *With regard to the drive FONN (7) and the response FONN (8). The sliding mode controller (16) and the composite learning law (26) guarantee that both the synchronization error $e(t)$ and the parameter estimation error $\tilde{\theta}(t)$ converge to zero asymptotically.*

Proof. Let the Lyapunov function be (20), and its derivative be (21). Putting (26) into (22), then (22) becomes

$$\begin{aligned}\dot{V}(t) &\leqslant -\lambda\sum_{i=1}^{n} S_i^2(t) + \sum_{i=1}^{n}\delta_i\psi_i(\zeta(t))\tilde{\theta}^T(t)S_i(t)\\ &\quad -\tfrac{1}{\gamma}\left[\gamma\sum_{i=1}^{n}\delta_i\psi_i(\zeta(t))S_i(t) + \gamma\sum_{i=1}^{n}\omega\epsilon_i(t)\right]\tilde{\theta}^T(t),\\ &= -\lambda\sum_{i=1}^{n} S_i^2(t) - \sum_{i=1}^{n}\omega\tilde{\theta}^T(t)\epsilon_i(t).\end{aligned} \tag{36}$$

Substituting (34) into (36) yields

$$\begin{aligned}\dot{V}(t) &\leqslant -\lambda\sum_{i=1}^{n} S_i^2(t) - \sum_{i=1}^{n}\omega\tilde{\theta}^T(t)\left[h_i(\zeta(t))\hat{\theta}(t) - \varepsilon_i(t)\right],\\ &= -\lambda\sum_{i=1}^{n} S_i^2(t) - \sum_{i=1}^{n}\omega\tilde{\theta}^T(t)\left[h_i(\zeta(t))\hat{\theta}(t) - h_i(\zeta(t))\theta\right],\\ &= -\lambda\sum_{i=1}^{n} S_i^2(t) - \sum_{i=1}^{n}\omega\tilde{\theta}^T(t)h_i(\zeta(t))\tilde{\theta}(t),\\ &\leqslant -\lambda\sum_{i=1}^{n} S_i^2(t) - n\omega v\tilde{\theta}^T(t)\tilde{\theta}(t),\\ &\leqslant -\upsilon V(t),\end{aligned} \tag{37}$$

where $\upsilon = \min\{2\lambda, 2n\gamma v\omega\}$. Therefore, both the synchronization error $e(t)$ and the parameter estimation error $\tilde{\theta}(t)$ tend to zero asymptotically. This ends the proof of Theorem 2. □

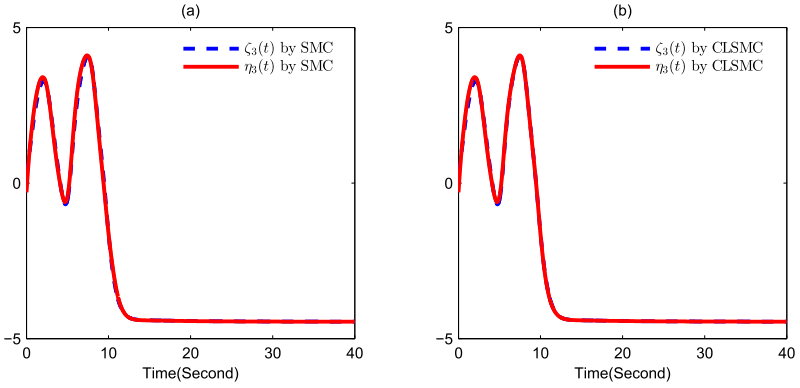

Fig. 7. Synchronization between $\zeta_3(t)$ and $\eta_3(t)$ for SMC and CLSMC.

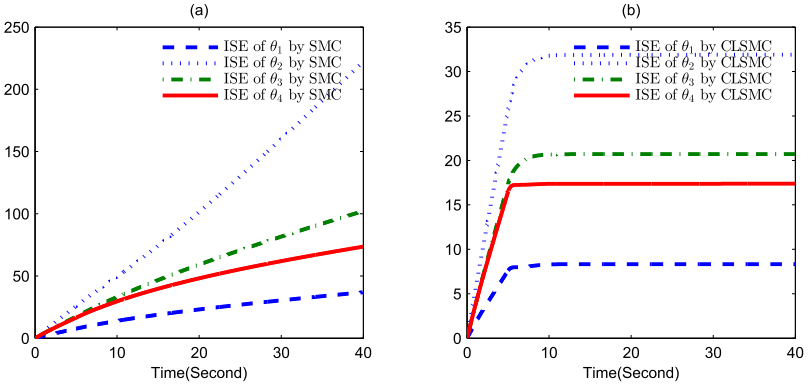

Fig. 8. ISE of parameters for SMC and CLSMC.

Remark 4. The SMC and CLSMC introduced in this article use the same controller (16). In terms of the advantages and disadvantages, the CLSMC which uses composite learning law (26) has the following merits. (1) In the adaptive SMC, only instantaneous data is applied to update $\hat{\theta}(t)$. However, in the CLSMC, all data recorded on interval $[t-\varsigma_0, t]$ is utilized. That is, the CLSMC method has remember ability, and the SMC method can be seen as a special case of the CLSMC (i.e., $\varsigma_0 = 0$). (2) In the CLSMC approach, the synchronization error $e(t)$ and the parameter estimation error $\tilde{\theta}(t)$ asymptotically approaching zero can be ensured under the IE condition, while only the $e(t)$ asymptotically approaching zero can be guaranteed under the PE condition in the adaptive SMC method. (3) Noting that the two methods, i.e., SMC and CLSMC, use the same controller (16), they will consume similar control energy in the same circumstance. However, in terms of control ability, the CLSMC approach has better control performance than the SMC method.

Remark 5. The advantage of the proposed CLSMC method over the traditional SMC method is obvious. Although both methods use the same control input (16) and they both ensure that the synchronization error $e(t)$ tends to zero, the PE condition must be satisfied to drive the synchronization error converges to zero in the SMC, while in the CLSMC, only the IE condition should be fulfilled. The CLSMC method uses the composite learning law (26) to update the estimation of θ. Compared with the SMC method using the adaptive law (17), the CLSMC method can obtain an accurate estimation of θ. This advantage of the proposed CLSMC method is proved in the proof of Theorem 2. In addition, through the comparison of ISE and MSE under the two methods in the simulation results of the next section, it can be concluded that the proposed CLSMC method has better control performance than the SMC method, although these two methods use similar control energy.

Simulation example

The drive FONN is given by

$$\begin{cases} D_t^{\alpha}\zeta_1(t) = -\zeta_1(t) + 2\tanh\zeta_1 - 1.2\tanh\zeta_2 + \psi_1^T(\zeta(t))\theta, \\ D_t^{\alpha}\zeta_2(t) = -\zeta_2(t) + 2\tanh\zeta_1 + 1.71\tanh\zeta_2 + 1.15\tanh\zeta_3 + \psi_2^T(\zeta(t))\theta, \\ D_t^{\alpha}\zeta_3(t) = -\zeta_3(t) - 4.75\tanh\zeta_1 + 1.1\tanh\zeta_3 + \psi_3^T(\zeta(t))\theta, \end{cases} \tag{38}$$

and the response FONN is

$$\begin{cases} D_t^{\alpha}\eta_1(t) = -\eta_1(t) + 2\tanh\eta_1 - 1.2\tanh\eta_2 + u_1(t), \\ D_t^{\alpha}\eta_2(t) = -\eta_2(t) + 2\tanh\eta_1 + 1.71\tanh\eta_2 + 1.15\tanh\eta_3 + u_2(t), \\ D_t^{\alpha}\eta_3(t) = -\eta_3(t) - 4.75\tanh\eta_1 + 1.1\tanh\eta_3 + u_3(t). \end{cases} \tag{39}$$

In the drive FONN system (38), when $\theta = [0,0,0,0]^T$ and $H_i = 0$, it becomes a chaotic system. The dynamical behavior of (38) with $\theta = [0,0,0,0]^T$ and $\alpha = 0.95$ is shown in Fig. 2.

The initial value of the drive FONN is $\zeta_0 = [-0.3, 0.4, 0.3]^T$ and the initial value of the response FONN is $\eta_0 = [0.3, -0.4, -0.3]^T$. The basis functions are set to be $\psi_1(\zeta(t)) = [0.25, 0.5\tanh\zeta_1, 0.5\sin(\zeta_1\zeta_2), 0.5\tanh(\zeta_1\zeta_3)]^T$, $\psi_2(\zeta(t)) = [0.5\sin(\zeta_1\zeta_2), 0.5\tanh\zeta_2, 0.5\sin\zeta_2, 0.5\tanh\zeta_3]^T$, $\psi_3(\zeta(t))$

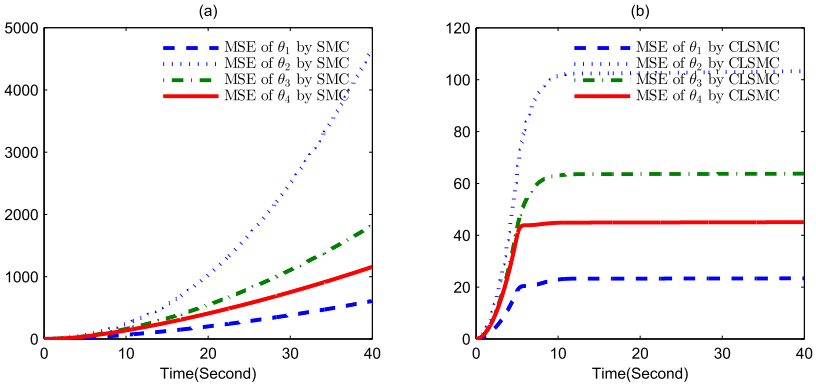

Fig. 9. MSE of parameters for SMC and CLSMC.

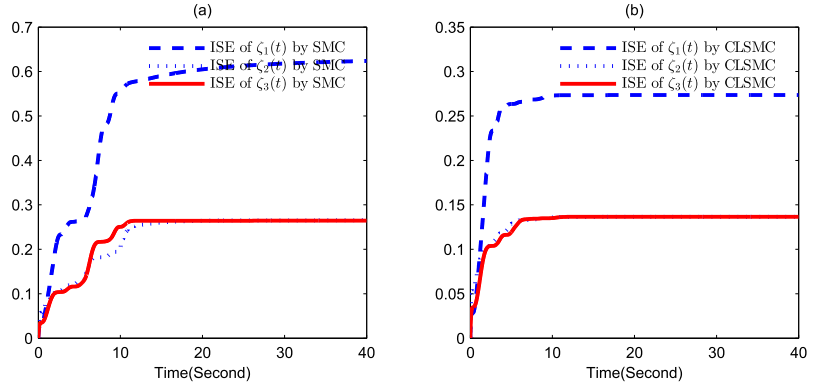

Fig. 10. ISE of state variables for SMC and CLSMC.

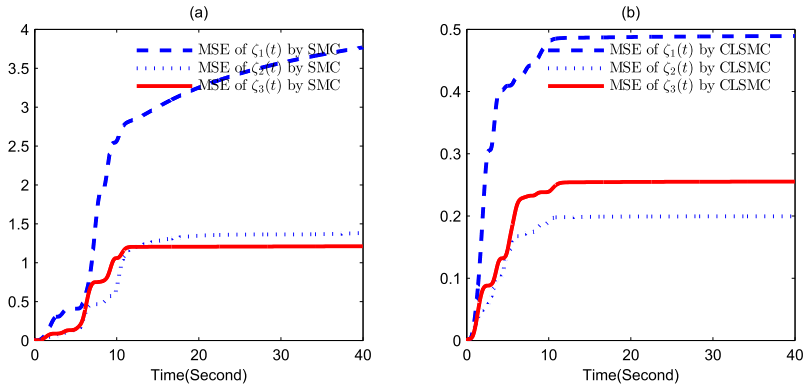

Fig. 11. MSE of state variables for SMC and CLSMC.

Table 1
The ISE and MSE for SMC and CLSMC.

Variable	ISE for SMC	ISE for CLSMC	MSE for SMC	MSE for CLSMC
θ_1	36.91	8.33	609.66	23.36
θ_2	222.13	31.90	4673.20	103.29
θ_3	102.12	20.71	1823.30	63.72
θ_4	73.55	17.38	1157.00	45.02
$\zeta_1(t)$	0.62	0.27	3.77	0.49
$\zeta_2(t)$	0.27	0.14	1.38	0.20
$\zeta_3(t)$	0.26	0.14	1.21	0.26

$= [0.5\cos\zeta_3, 0.05, 0.5\tanh\zeta_1, 0.5\sin\zeta_2]^T$, and $\theta = [0.3, -0.2, 0.9, -0.7]^T$. The parameters of the controller are designed as $\gamma = 1, \delta_1 = \delta_2 = \delta_3 = 1, \omega = 1, \beta = 100, \varsigma_0 = 5, \lambda = 5$.

In Figs. 3–11 and Table 1, we compare the SMC method and the CLSMC method in detail. The control inputs of the two control methods are shown in Fig. 3 (a), (b), (c), and the sliding surfaces are given in Fig. 3 (d), (e), (f). The estimation of θ is presented in Fig. 4. The synchronization performance of $\zeta_1(t), \zeta_2(t), \zeta_3(t)$ by using the two control methods are indicated in Fig. 5, Fig. 6 and Fig. 7, respectively. The ISE and MSE of parameters and state variables for SMC and CLSMC are shown in Figs. 8–11. Finally, the values of ISE and MSE at $t = 40$ (s) under the SMC method and the CLSMC method are given in Table 1. From these simulation results, we have the following concoctions. (1) It can be seen from dynamics of sliding surfaces and the synchronization between the drive FONN and the response FONN under SMC and CLSMC, the convergence speed of synchronization error $e_1(t)$ and $e_2(t)$ is faster under CLSMC than under SMC (although the rate at which $e_3(t)$ approaches zero is similar in both methods). It is commonly recognized that the smaller of the ISE and MSE, the higher the accuracy of the estimation, therefore, the convergence rate of $e_1(t)$ and $e_2(t)$ under the CLSMC is faster than that under the SMC. It can be verified that in Fig. 10 and Fig. 11 the ISE and MSE of θ and $\zeta(t)$ by using the CLSMC are less than by using the SMC. In Table 1, the ISE and MSE of the two control methods when $t = 40$ (s) are given, from which similar conclusions can be obtained. (2) From Fig. 8 (b) and Fig. 9 (b), it can be seen that ISE and MSE in the CLSMC method finally approach a certain value, and the value of ISE and MSE at $t = 40$(s) obtained from Table 1 is very small, which indicates that the parameters in the CLSMC have been accurately estimated. On the contrary, in Fig. 8 (a) and Fig. 9 (a), we can see that ISE and MSE under the SMC are always on the rise and the values of ISE and MSE at $t = 40$(s) obtained from Table 1 are very large, which represent that the SMC method does not have the ability to accurately estimate parameters. (3) In terms of control performance, by comparing the ISE and MSE of the two control methods in Figs. 8–11 and Table 1. We can figure out the ISE and MSE by using the CLSMC are less than by using the SMC, which is the CLSMC technique that has a better control performance than the SMC and can stabilize the system in a short time. (4) It should be emphasized that the two control methods use the same control signal, then they consume similar control energy (which can be seen in Fig. 3(a), (b), (c)). However, the CLSMC technique obtain better synchronization performance than the SMC method.

Conclusions

This paper presents a composite learning sliding mode synchronization method for chaotic FONNs with unmatched unknown parameter. By using the traditional SMC method, the convergence of the synchronization error can be guaranteed under the PE condition. Then, a CLSMC method is proposed, and it is proved that the proposed CLSMC method can achieve the accurate estimation of unknown parameter and ensures that the parameters converges to zero asymptotically under an IE condition that is lower than the PE condition. In addition, by comparing the ISE and MSE under the two methods, it is concluded that the CLSMC method can not only achieve accurate parameter estimation without the PE condition, but also has better control performance than the SMC approach. One of the future work will focus on how to design composite learning adaptive sliding mode synchronization of uncertain FONNs.

Declaration of Competing Interest

The authors declare that they have no known competing financial interests or personal relationships that could have appeared to influence the work reported in this paper.

Compliance with ethics requirements

This article does not contain any studies with human or animal subjects.

Acknowledgments

This work is supported by the National Natural Science Foundation of China (61967001 and 11771263), the Guangxi Natural Science Foundation (2018JJA110113), and the Xiangsihu Young Scholars Innovative Research Team of Guangxi University for Nationalities (2019RSCXSHQN02).

References

[1] Radwan AG, Soliman AM, Elwakil AS. Design equations for fractional-order sinusoidal oscillators: Four practical circuit examples. Int J Circuit Theory Appl 2008;36(4):473–92.
[2] Radwan AG, Salama KN. Fractional-order RC and RL circuits. Circuits Syst Signal Process 2012;31(6):1901–15.
[3] Podlubny I. Fractional differential equations: an introduction to fractional derivatives, fractional differential equations, to methods of their solution and some of their applications, vol. 198. Elsevier; 1998.
[4] Shen J, Lam J. Stability and performance analysis for positive fractional order systems with time-varying delays. IEEE Trans Autom Control 2016;61(9):2676–81.
[5] Liu H, Li S, Wang H, Sun Y. Adaptive fuzzy control for a class of unknown fractional-order neural networks subject to input nonlinearities and dead-zones. Inf Sci 2018;454–455:30–45.
[6] Li M, Wang J. Exploring delayed mittag-leffler type matrix functions to study finite time stability of fractional delay differential equations. Appl Math Comput 2018;324:254–65.
[7] Tsirimokou G, Psychalinos C. Ultra-low voltage fractional-order differentiator and integrator topologies: an application for handling noisy ecgs. Analog Integr Circ Sig Process 2014;81(2):393–405.
[8] Arena P, Caponetto R, Fortuna L, Porto D. Bifurcation and chaos in noninteger order cellular neural networks. Int J Bifur Chaos 1998;8:1527–39.
[9] Petras I. A note on the fractional-order cellular neural networks. In: 2006 IEEE international joint conference on neural network proceedings. IEEE; 2006. p. 1021–4.
[10] Wu R, Lu Y, Chen L. Finite-time stability of fractional delayed neural networks. Neurocomputing 2015;149:700–7.
[11] Huang H, Huang T, Chen X. A mode-dependent approach to state estimation of recurrent neural networks with markovian jumping parameters and mixed delays. Neural Netw 2013;46:50–61.
[12] Arena P, Fortuna L, Porto D. Chaotic behavior in noninteger-order cellular neural networks. Phys Rev E 2000;61(1):776.
[13] Arefeh B, Mohammad BM. Fractional-order hopfield neural networks. In: International conference on advances in neuro-information processing. Berlin: Springer; 2009. p. 883–90.
[14] Chen L, Qu J, Chai Y, Wu R, Qi G. Synchronization of a class of fractional-order chaotic neural networks. Entropy 2013;15(8):3265–76.
[15] Ha S, Liu H, Li S, Liu A. Backstepping-based adaptive fuzzy synchronization control for a class of fractional-order chaotic systems with input saturation. Int J Fuzzy Syst 2019;21(12):1571–84.
[16] Ha S, Liu H, Li S. Adaptive fuzzy backstepping control of fractional-order chaotic systems with input saturation. J Intell Fuzzy Syst 2019;37(5):6513–25.
[17] Liu H, Pan Y, Cao J, Zhou Y, Wang H. Positivity and stability analysis for fractional-order delayed systems: a T-S fuzzy model approach. IEEE Trans Fuzzy Syst doi: 10.1109/TFUZZ.2020.2966420.
[18] Liu H, Wang H, Cao J, Alsaedi A, Hayat T. Composite learning adaptive sliding mode control of fractional-order nonlinear systems with actuator faults. J Franklin Inst 2019;356(16):9580–99.
[19] Furuta K. Sliding mode control of a discrete system. Syst Control Lett 1990;14(2):145–52.
[20] Yang J, Li S, Yu X. Sliding-mode control for systems with mismatched uncertainties via a disturbance observer. IEEE Trans Ind Electron 2012;60(1):160–9.
[21] Liu X, Su X, Shi P, Shen C, Peng Y. Event-triggered sliding mode control of nonlinear dynamic systems. Automatica 2020;112:108738.
[22] Xiong L, Li P, Wu F, Ma M, Khan MW, Wang J. A coordinated high-order sliding mode control of dfig wind turbine for power optimization and grid synchronization. Int J Electr Power Energy Syst 2019;105:679–89.
[23] Belkhatir Z, Laleg-Kirati TM. High-order sliding mode observer for fractional commensurate linear systems with unknown input. Automatica 2017;82:209–17.
[24] Vahidi-Moghaddam A, Rajaei A, Ayati M. Disturbance-observer-based fuzzy terminal sliding mode control for mimo uncertain nonlinear systems. Appl Math Model 2019;70:109–27.
[25] Song C, Fei S, Cao J, Huang C. Robust synchronization of fractional-order uncertain chaotic systems based on output feedback sliding mode control. Mathematics 2019;7(7):599.
[26] Liu H, Pan Y, Jinde C, Hongxing W, Yan Z. Adaptive neural network backstepping control of fractionial-order nonlinear systems with actuator faults. IEEE Trans Neural Netw Learn Syst doi: 10.1109/TNNLS.2020.2964044.
[27] Slotine J-JE, Li W. Composite adaptive control of robot manipulators. Automatica 1989;25(4):509–19.
[28] Pan Y, Sun T, Yu H. Composite adaptive dynamic surface control using online recorded data. Int J Robust Nonlinear Control 2016;26(18):3921–36.
[29] Wang L, Basin MV, Li H, Lu R. Observer-based composite adaptive fuzzy control for nonstrict-feedback systems with actuator failures. IEEE Trans Fuzzy Syst 2017;26(4):2336–47.
[30] Jana S, Bhat MS. Composite adaptive control using output feedback and application to micro air vehicle. In: Control systems (SICE ISCS), 2017 SICE international symposium on. IEEE; 2017. p. 1–8.
[31] Phu DX, Huy TD, Mien V, Choi S-B. A new composite adaptive controller featuring the neural network and prescribed sliding surface with application to vibration control. Mech Syst Signal Process 2018;107:409–28.
[32] Liu Y-J, Tong S. Barrier lyapunov functions-based adaptive control for a class of nonlinear pure-feedback systems with full state constraints. Automatica 2016;64:70–5.
[33] Pan Y, Sun T, Liu Y, Yu H. Composite learning from adaptive backstepping neural network control. Neural Netw 2017;95:134–42.
[34] Xu B, Sun F, Pan Y, Chen B. Disturbance observer based composite learning fuzzy control of nonlinear systems with unknown dead zone. IEEE Trans Syst Man Cybernet Syst 2017;47(8):1854–62.
[35] Pan Y, Yu H. Composite learning robot control with guaranteed parameter convergence. Automatica 2018;89:398–406.
[36] Pan Y, Yu H. Composite learning from adaptive dynamic surface control. IEEE Trans Autom Control 2016;61(9):2603–9.
[37] Liu H, Pan Y, Cao J. Composite learning adaptive dynamic surface control of fractional-order nonlinear systems. IEEE Trans. Cybernet. doi: 10.1109/TCYB.2019.2938754.
[38] Farrell JA, Polycarpou MM. Adaptive approximation based control: unifying neural, fuzzy and traditional adaptive approximation approaches, vol. 48. John Wiley & Sons; 2006.